applied sciences

MDPI

Article

Research on the Exterior Mortar of the Corbii de Piatra Cave Church

Flavio Nicolae Finta [1], Marioara Abrudeanu [1,*], Denis Aurelian Negrea [2,3,*], Izabela Victoria Maris [4], Sorin Georgian Moga [2,3], Cristian Manailescu [5], Corina Anca Simion [5], Maria Valentina Luca Ilie [5], Mircea Ionut Petrescu [6], Magdalena Ecaterina Modan [2,3], Florentina Popa [3,7], Dorin Grecu [8], Daniela Gheorghita Giugea [8], Ionela Cristina Gheorghe [1], Tiberius Nicolae Duta [1] and Marius Lungescu [1]

1 Doctoral School of Materials Science and Engineering, National University of Science and Technology POLITEHNICA Bucharest, Splaiul Independentei nr. 313, District 6, 060042 Bucharest, Romania; nicolae.finta@stud.sim.upb.ro (F.N.F.); ionela.gheorghe1709@stud.sim.upb.ro (I.C.G.); nicusor.duta2012@stud.sim.upb.ro (T.N.D.); marius.lungescu@stud.sim.upb.ro (M.L.)
2 Faculty of Mechanics and Technology, Pitesti University Centre, National University of Science and Technology POLITEHNICA Bucharest, 110040 Pitesti, Romania; sorin_georgian.moga@upb.ro (S.G.M.); ecaterina.modan@upb.ro (M.E.M.)
3 Regional Center of Research & Development for Materials, Processes and Innovative Products Dedicated to the Automotive Industry (CRCD-AUTO), Pitesti University Centre, National University of Science and Technology POLITEHNICA Bucharest, 110040 Pitesti, Romania; florentina.popa1702@upb.ro
4 Department of Mineralogy, Faculty of Geology and Geophysics, University of Bucharest, 1 N. Bălcescu Ave., 011401 Bucharest, Romania; izabela@contentlogic.ro
5 Horia Hulubei National Institute for R&D in Physics and Nuclear Engineering (IFIN-HH), 30 Reactorului St., P.O. Box–MG-06, 077125 Magurele, Romania; cristian.manailescu@nipne.ro (C.M.); anke@nipne.ro (C.A.S.); maria.ilie@nipne.ro (M.V.L.I.)
6 Department of Engineering and Management of Metallic Materials Casting, Faculty of Materials Science and Engineering, National University of Science and Technology POLITEHNICA Bucharest, Splaiul Independentei nr. 313, Sector 6, 060042 Bucharest, Romania; ionut.petrescu@upb.ro
7 Faculty of Sciences, Physical Education and Computer Science, Pitesti University Centre, National University of Science and Technology POLITEHNICA Bucharest, 060042 Bucharest, Romania
8 Faculty of Theology, Letters, History and Arts, Pitesti University Centre, National University of Science and Technology POLITEHNICA Bucharest, 110040 Pitesti, Romania; dorin_grecuro@upb.ro (D.G.); gheorghita.giugea@upb.ro (D.G.G.)
* Correspondence: abrudeanu@gmail.com (M.A.); aurelian.negrea@upb.ro (D.A.N.)

Abstract

The deterioration of the mural paintings in the rock-hewn Church of Corbii de Piatră is primarily caused by water infiltration. The transport of water through the sandstone of the northern wall and its subsequent penetration into the fresco layer, together with the associated deterioration processes, were investigated in a previously published study. The present study, conducted during the preliminary stage of the restoration process of the rock-hewn Church of Corbii de Piatră, aims to characterize the exterior mortar, which is intended to protect the sandstone wall against water ingress originating from precipitation and from the nearby watercourse, Cascade Stream. The interdisciplinary characterization, which included mineralogical, macro- and microstructural investigations, elemental chemical analyses, and qualitative phase analyses, provided information on the composition and structure of the mortar. The study revealed the presence of large cracks crossing the exterior mortar layer, which developed as a result of repeated freeze–thaw cycles and caused the detachment of portions of the mortar, as well as internal compactness defects, pores, and fine cracks. The mortar has a particular composition, characterized by the presence of numerous phases highly enriched in carbon, aluminosilicates or iron silicates, and aggregates with a high iron content. The structure with large aggregates is characteristic of ancient settling mortars. Radiocarbon dating suggests that the mortar covering on the northern exterior wall was hardened after the second half of the 17th century AD. The most probable interval

Check for updates

Academic Editor: Weichung Yeih

Received: 14 October 2026
Revised: 20 November 2026
Accepted: 23 November 2026
Published: 27 November 2026

Copyright: © 2026 by the authors. Licensee MDPI, Basel, Switzerland. This article is an open access article distributed under the terms and conditions of the Creative Commons Attribution (CC BY) license.

is calAD 1723 (50.1%) to 1814. This range was further narrowed down to the late 18th—early 19th century, based on references in historical documents and by correlating it with a previous radiocarbon date obtained for the wooden table from the refectory, which was made during the same period. The advanced characterization of the exterior mortar, together with the results of the previous study on the deterioration of the mural paintings at Corbii de Piatră, provides essential data for supporting restoration and conservation interventions. The penetration of meteoric water through the exterior mortar towards the sandstone wall could be avoided or at least reduced by using an exterior settling mortar with large aggregates. Furthermore, radiocarbon dating contributes to a better understanding of the monument's conservation history.

Keywords: historical mortar; meteoric water infiltration; mortar degradation; intedisciplinary characterization; radiocarbon dating

1. Introduction

A historic monument dating back to the 13th–14th centuries, the Corbii de Piatră Church is considered the first painted cave church in Romania. Carved into a sandstone wall, the church has unique architectural features, including a nave with two altars (Figure 1). Historical evidence suggests that Basarab I the Founder (c. 1310–1352) was responsible for its construction. Iconographic studies support this attribution, with a portrait in the church's fresco possibly representing the earliest known fresco depiction of Basarab I [1].



Figure 1. Corbii de Piatră Church (photo from the personal archive of F.N.F.).

Previous studies [2,3] highlighted the impact of infiltrating water on degradation processes affecting the microstructure, chemical composition, and phase composition, and

consequently the adhesion of the fresco mortars to the sandstone wall (Figure 2). One of the causes of the deterioration could be water infiltration through the exterior mortar.

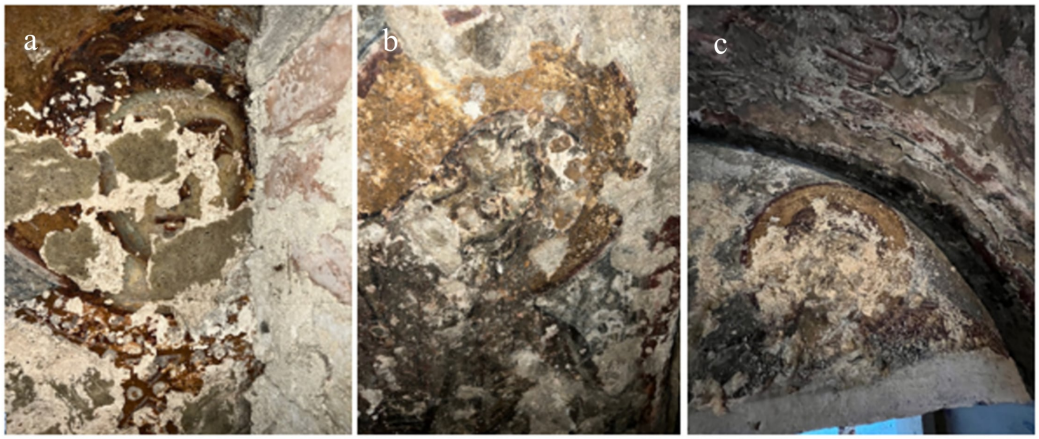

Figure 2. Degradation of the fresco painting in the Corbii de Piatră Church. (**a**,**b**) Areas of fresco deterioration on the north wall, approximately 170 cm above floor levels; (**c**) area of deterioration in the vicinity of the altar (personal archive photo FNF).

Meteoric water is collected from the sandstone slope in which the church is carved by the Cascade Stream, which is at the same level as the church and flows along the northern wall.

A recent study on the interior fresco established through radiocarbon dating that the investigated areas belong to the early stages of painting of the interior of the cave church: the southern wall, during the time of Voivode Basarab I the Founder (1310–1352) and the northern wall, in the second half of the 14th century, with the latter having long been affected by water seepage. These results are supported by historical documents and specialized publications [2–9].

Regarding the northern wall, documents state that the church's original entrance was located here and that it was likely walled up during the reign of Neagoe Basarab (1512–1521) [8]. In the same publication, pages 76, 77, a document from 1856 notes that, subsequently, the interior northern wall was severely damaged by dampness. An opening into the narthex was created in the southern wall. The church underwent repairs in 1809. In 1814, a women's vestibule (*tinda*) was added in this area, thereby reducing the size of the refectory (*trapezaria*). On this occasion, modifications were also made to the western wall (Figure 1), involving the remodeling of the original windows. It is recorded that this wall collapsed following an earthquake in 1887 and was subsequently rebuilt. No interventions were recorded regarding the northern wall.

Concerning the table in the refectory, although local legends place it at the time of Neagoe Basarab (1512–1521), himself having a role in the development of the monastic community, it was nevertheless given a radiocarbon date with a dominant interval calAD 1725 (51.1%) 1813 [10]. It was present in 1856 and mentioned in the previously cited document.

This study expands upon previous multidisciplinary research [2–10] through an advanced characterization of the exterior northern wall mortar, presumed to be older than the late 19th-century reconstructions, with the aim of highlighting its age, composition, contribution to the protection of the wall and, ultimately, the interior fresco paintings.

In this way, the study of the mortar will complete the previous publications on this unique rock complex in Romania and will be able to be included in the archaeometric contributions next to those already published in this region of Europe [11–16].

2. Materials and Methods

For mortar characterization, large mortar samples were collected from three locations on the northern wall (Figure 3), which is exposed to water supplied by the Cascade Stream. Two samples were taken from areas exhibiting cracks (Figure 3a,b), while the third was collected from an area showing mortar detachment (Figure 3c). The samples were collected with the full thickness of the mortar layer preserved. They were subsequently sectioned using an abrasive cutting disk, then embedded in conductive resin and prepared by mechanical grinding for macroscopic and microscopic analyses. The samples intended for X-ray diffraction analysis were ground into powder using a mortar and pestle.

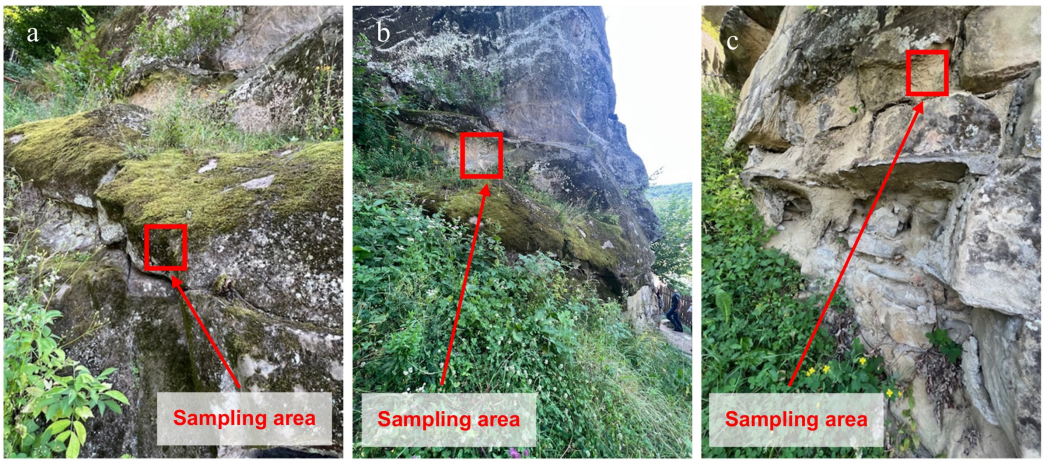

Figure 3. The northern wall of the Corbii de Piatră Church from which mortar samples were taken: (**a**) major crack in the plaster on the east wall, (**b**) areas of mortar exhibiting deep cracks, (**c**) area of mortar detachment (personal archive photo FNF).

Macroscopic analysis of the mortar samples was performed both with the naked eye and using an Olympus stereomicroscope (Olympus Corporation, Tokyo, Japan). Optical microscopy (OM) characterization was carried out under polarized light using a Zeiss Observer A1m optical microscope (Carl Zeiss Microscopy GmbH, Jena, Germany), which allows magnifications of up to 1000×, visualization in bright-field, dark-field, and polarized light, as well as image acquisition using a Canon camera (Canon Inc., Tokyo, Japan).

The particle size analysis was performed on two polished samples using an Olympus SZX2-ILLT binocular magnifier (Olympus Corporation, Tokyo, Japan), equipped with an Olympus U-CMAD3 photo camera (Olympus Corporation, Tokyo, Japan). The particles were measured using the QuickPhoto 3.2 (PROMICRA, s.r.o., Prague, Czech Republic) photo acquisition software [17–19].

Microscopic analysis by cathodoluminescence (CL) [20–23] was performed using a Nikon E400 optical microscope (Nikon, Tokyo, Japan), equipped with a cold-cathode cathodoluminescence device CL 8200 MK 3A (Cambridge Image Technology Ltd., Cambridge, UK). Images were captured using a COOLPIX 950 digital photomicrograph device (Nikon Corporation, Tokyo, Japan). The parameters employed for this technique included an average vacuum pressure of 0.5 Torr, an accelerating voltage of 15–17 kV, and a beam current of 350–400 µA, in accordance with applicable standards [24–27]. The interpretation of cathodoluminescence results is qualitative in nature [20–23].

Characterization of the mortars by scanning electron microscopy coupled with energy-dispersive spectroscopy (SEM–EDS) was conducted using a HITACHI SU5000 electron microscope, equipped with a backscattered electron detector and an EDS module for elemental analysis (Hitachi Group, Tokyo, Japan) [28–37].

X-ray diffraction (XRD) analysis was used to complete the identification of crystalline phases within the mortar [38–43]. XRD measurements were carried out using an Rigaku Ultima IV system (Rigaku Corporation, Tokyo, Japan), equipped with a Cu X-ray tube (Kα = 0.154051 nm), operating in a 2θ range of 20–70°, with a step size of 0.05° and a scanning speed of 2 deg/min. Qualitative phase analysis was performed using PDXL2 software (Rigaku Corporation, Japan) and the PDF-5+ 2024 database (International Centre for Diffraction Data).

The radiocarbon dating of the exterior mortar was carried out at the RoAMS Laboratory of the in Horia Hulubei National Institute for R&D in Physics and Nuclear Engineering (IFIN-HH) [44–52].

In the radiocarbon dating laboratory, alongside the material analyses, two aspects were monitored to help quantify the degree of carbonation [45,46]: the reaction with a 2% phenolphthalein-in-alcohol solution of raw material and, finally, the degree of rehydration of the sub-micron deposit on the watch glass—a phenomenon occurring after the deposit had been vacuum-dried to recover the calcite before graphitization, using the same color test.

In the initial material, no pink coloration—characteristic of a basic environment—appeared after the tested portion of the sample was immersed in ultrapure water. The absence of portlandite was indicated by the formation of a sub-micron yellowish-white deposit on the watch glass (if present, portlandite would immediately absorb moisture from the atmospheric air, resulting in the formation of a translucent gel). Taking a small portion, treating it with phenolphthalein, and immersing it in water did not result in the solution becoming colored.

Following an initial negative phenolphthalein test, the sub-micron fraction was extracted from 15 g of bulk mortar via sedimentological separation and sequential centrifugation. This method—now the standard procedure at RoAMS—allows for the recovery of the sub-micron fraction, which contains calcite formed at the time the protective lime plaster layer hardened on the stone wall [47–52]. Air lime plaster can be dated provided that the binder is $Ca(OH)_2$, which carbonates into $CaCO_3$; a well-preserved fraction of primary binder calcite can be isolated; no significant secondary recrystallization has occurred; and hydraulic or pozzolanic reactions are absent. Furthermore, there must be no unburnt geological limestone—whether naturally present or intentionally added—that would significantly lower the radiocarbon age (this was not the case for this sample). After recovering approximately 25 mg of a whitish-yellow deposit from the watch glass—obtained by drying the final solution in a vacuum oven—the material, denoted with the lab code 3447.173, is graphitized using a Carbon Handling System coupled with an AGE 3 system. The carbon, deposited intimately onto an iron catalyst, is then loaded into a cathode and measured via the AMS method using a 1 MV HVEE Cockcroft–Walton Tandetron accelerator.

Regarding the risk of contamination by much older or more recent carbon, the calibrated result was deemed consistent with historical and archaeological information. Preliminary tests also support the decision not to repeat the analyses—all the more so given that any intervention must be minimally invasive, considering the significance of the historical monument.

3. Experimental Results and Discussion

Visual inspection of the mortar on the northern exterior wall revealed the presence of cracks, most likely caused by freeze–thaw cycles resulting from the expansion of ice formed within the mortar pores and cracks. The samples were collected from the cracked areas (Figure 3a,b) and from an area where the mortar had become completely detached (Figure 3c). Specimens for macroscopic and microscopic analyses, X-ray diffraction and radiocarbon dating were cut from the collected samples using an abrasive cutting disk.

Macroscopic examination of the mortar samples in cross-section after cutting (Figure 4) revealed particles of different sizes, ranging from white to gray tones, as well as fine, bright white particles. The structure exhibits pores of various sizes, most of which are unconnected.



Figure 4. Macroscopic analysis of the mortar samples for different magnifications (**a**) 30×, (**b**) 20×, (**c**) 10×.

Optical microscopic analysis highlighted the morphology and varying sizes of the particles embedded in the lime matrix. The different nature of the particles is revealed. (Figures 5 and 6). The analyzed samples revealed sedimentary particles with different sizes, from very coarse to very fine arenites (Tables 1 and 2). In both samples, the dominant fraction is medium arenite (Figures 7 and 8). The standard deviation values suggest an arenitic mixture with poor sorting. The grains have angular, subangular and subrounded shapes, many of them being in point contact.

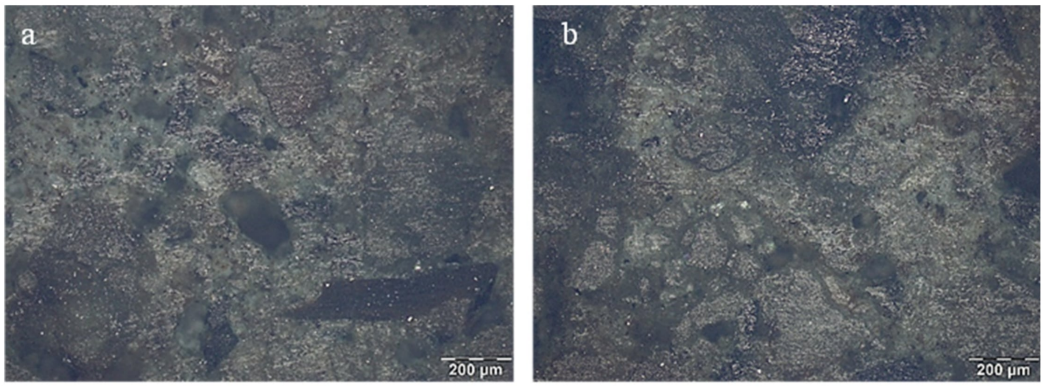

Figure 5. Microstructure determined by optical microscopy in white light for two different areas (**a**,**b**).

The granulometric analysis of Corbii de Piatra's external wall was performed by direct measurements on the polished sample, using an Olympus SZX2-ILLT binocular magnifier, equipped with an Olympus U-CMAD3 photo camera and using the QuickPhoto 3.2 photo acquisition software (Figure 7, Table 1).

Table 1. Statistical grain size analysis of the exterior mortar used at the cave complex at Corbii de Piatra.

Measurand	Number of Measure-ments	Minimal Value	Maximal Value	Average Value	Standard Deviation
Length	274	73 µm	1435 µm	399.0 µm	247.1 µm

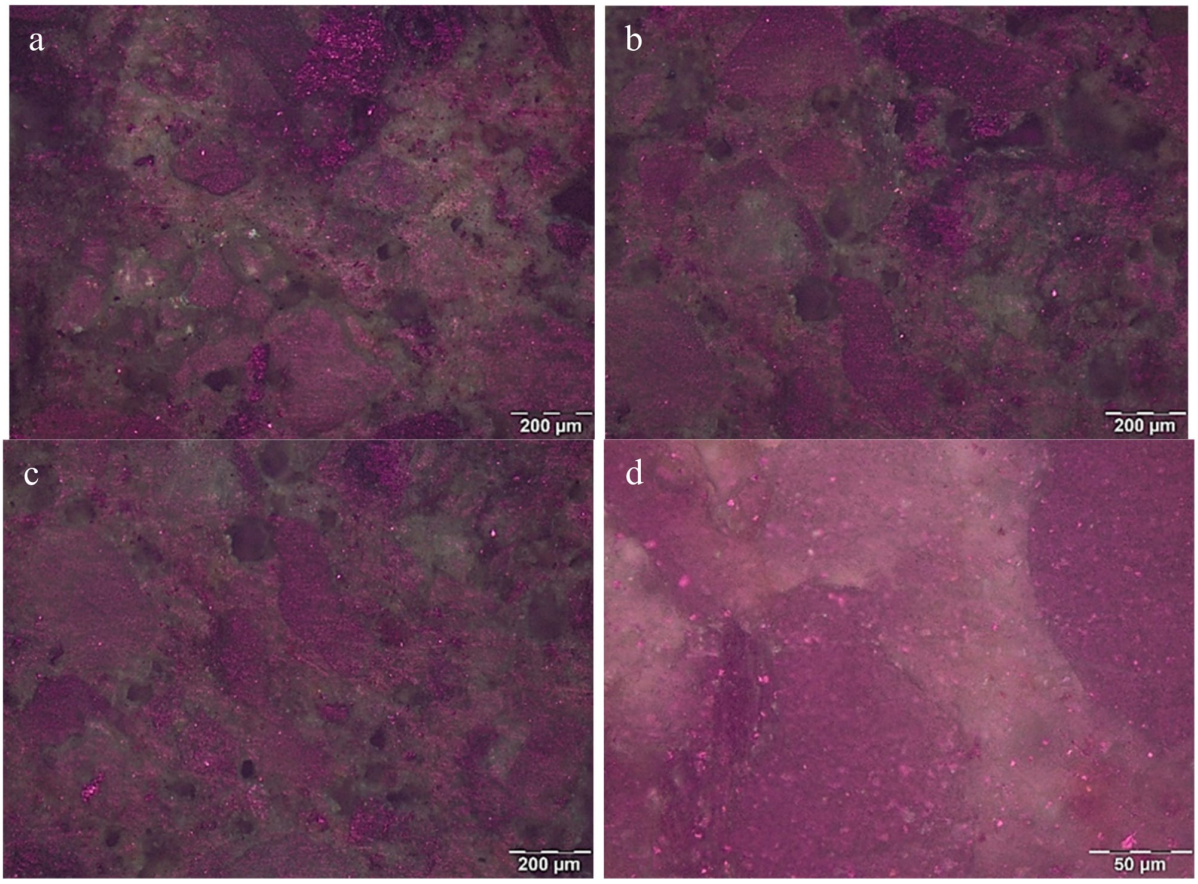

Figure 6. Microstructure observed by optical microscopy in polarized light. In all four areas investigated (**a**–**d**), the analyses highlighted the presence of fine, bright white particles.

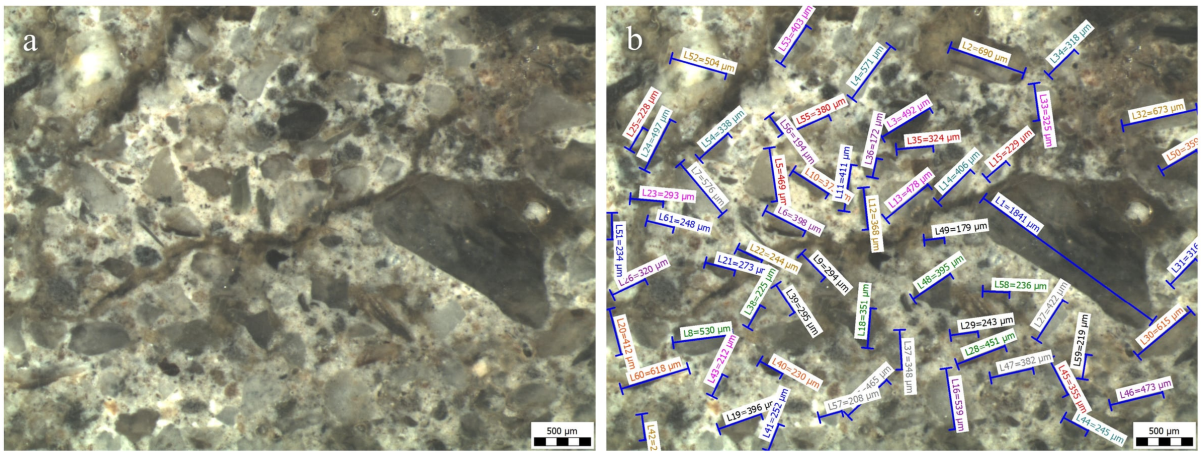

Figure 7. The polished sample which highlights (**a**) the granulometric distribution of the particles and (**b**) the same sample after measurements.

Table 2. Chemical composition of the mortar determined by SEM–EDS analysis at 13 measurement points.

Spectrum Label	Spectrum 1	Spectrum 2	Spectrum 3	Spectrum 4	Spectrum 5	Spectrum 6	Spectrum 7	Spectrum 8	Spectrum 9	Spectrum 10	Spectrum 11	Spectrum 12	Spectrum 13
C	16.01	8.92	7.92	10.17	80.18	30.85	9.34	8.68	54.78	23.48	10.95	7.23	15.71
O	38.85	51.62	46.18	42.30	16.34	37.47	30.79	38.64	27.84	44.41	43.11	35.98	36.27
Na		0.09	3.83	0.52	0.04	0.21	0.28	0.14	0.14		0.44	0.62	0.20
Mg	2.02		0.59		0.06	0.38	3.42	1.29	0.50			1.17	0.63
Al	8.56	0.21	11.85	8.61	0.19	1.23	6.58	3.71	2.20	0.17	8.60	11.21	0.93
Si	12.80	38.58	23.97	26.28	1.25	9.26	9.59	12.35	8.65	31.08	24.86	3.90	7.80
P							0.42		0.06				
S					0.05	0.20		0.10	0.13			0.07	0.11
K	0.06	0.07	4.19	10.95	0.04	0.34	0.57	0.12	0.65	0.09	10.11	0.35	
Ca	2.39	0.51	0.73	1.03	1.62	18.69	4.36	26.17	4.05	0.66	0.73	31.10	37.31
Ti								0.62	0.07			0.34	0.12
Mn	0.21						0.15	1.00				0.37	0.11
Fe	19.09		0.74	0.15	0.22	1.39	34.50	7.19	0.94	0.11	0.19	7.64	0.80
Ba											1.00		
Total	100.00	100.00	100.00	100.00	100.00	100.00	100.00	100.00	100.00	100.00	100.00	100.00	100.00

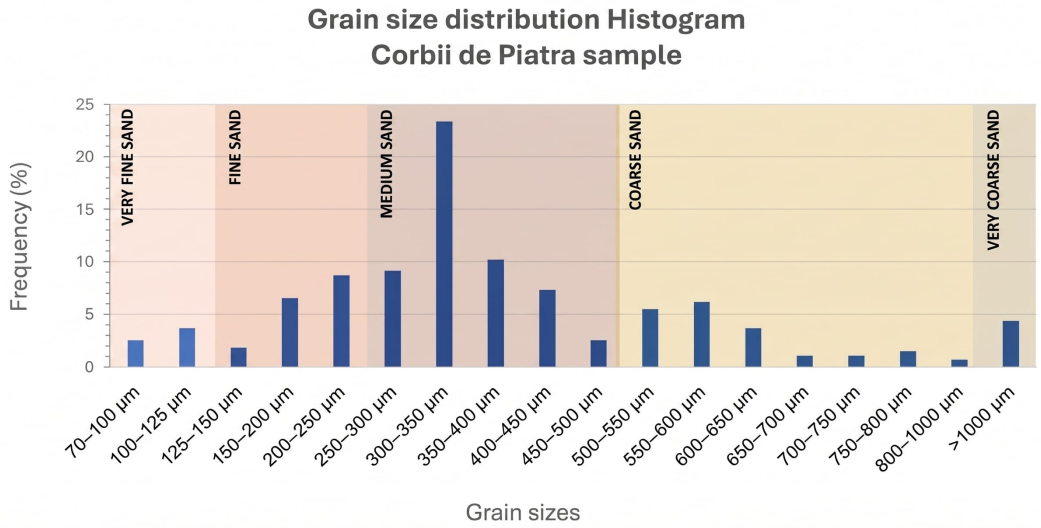

Figure 8. Grain size distribution of particles within mortar from Corbii de Piatră.

The granulometric values varied between 73 and 1435 µm, which corresponds to the granulometric classes from very fine to very coarse sand, with an average of 399.0 µm, specific to medium sand (after Udden Wentwort grain size scale, 1922 [27]).

The standard deviation value defines the degree of sorting of the material involved. The value of 247.1 µm (=2.02 Φ units) expresses a very poor sorting of the sedimentary material used in the mortar preparation.

The histograms below show the variation in the grain size distribution with the dominance of the medium arenite grain size class (Figure 8).

The mineralogical composition of the Corbii de Piatra CL sample is complex (Figure 9), consisting of particles with different mineralogies embedded in a fine, homogeneous brown-blackish non-luminescent matrix. Mineralogical composition is dominated by quartz, subordinate feldspar, metamorphic lithoclasts and rare carbonate grains. The quartz grains have different origins such as magmatic quartz with dull light blue luminescence, volcanic quartz with dull violet luminescence and hydrothermal quartz with dull brown luminescence. Feldspar grains are strongly luminescent with yellow-green or blue colors. Metamorphic rock fragments are found in small proportion, but they have the largest granulometry (very coarse sand). These grains have schistous structure and multiple luminescent colors (blue, gray, brown), specific to mica schists. Rarely fragments of carbonate rocks appear, with bright orange luminescence.

Vacuolar areas with irregular edges are distinguished, on which magnesian calcite has precipitated, having a bright luminescence of orange-reddish color.

Also, infiltrative pathways are observed, circulated by fluids rich in Ca^{2+}, Mg^{2+} and Mn^{2+} ions, with a luminescence signature specific to carbonate minerals (magnesian calcite) of bright orange-reddish luminescence color. In some places, bright red dolomite microcrystals are reported.

The granules are linked together by a fine, homogeneous, non-luminescent material, brown-blackish.

Morphological analysis of the cross-section by scanning electron microscopy (SEM) reveals grains with varying shapes, sizes, and contrast levels (Figure 10a,b,e), together with larger continuous regions characteristic of the mortar matrix, displaying different shades of gray (Figure 10c,d,f). In addition, white crystalline formations arranged in rosette-like structures can be observed (Figure 11).

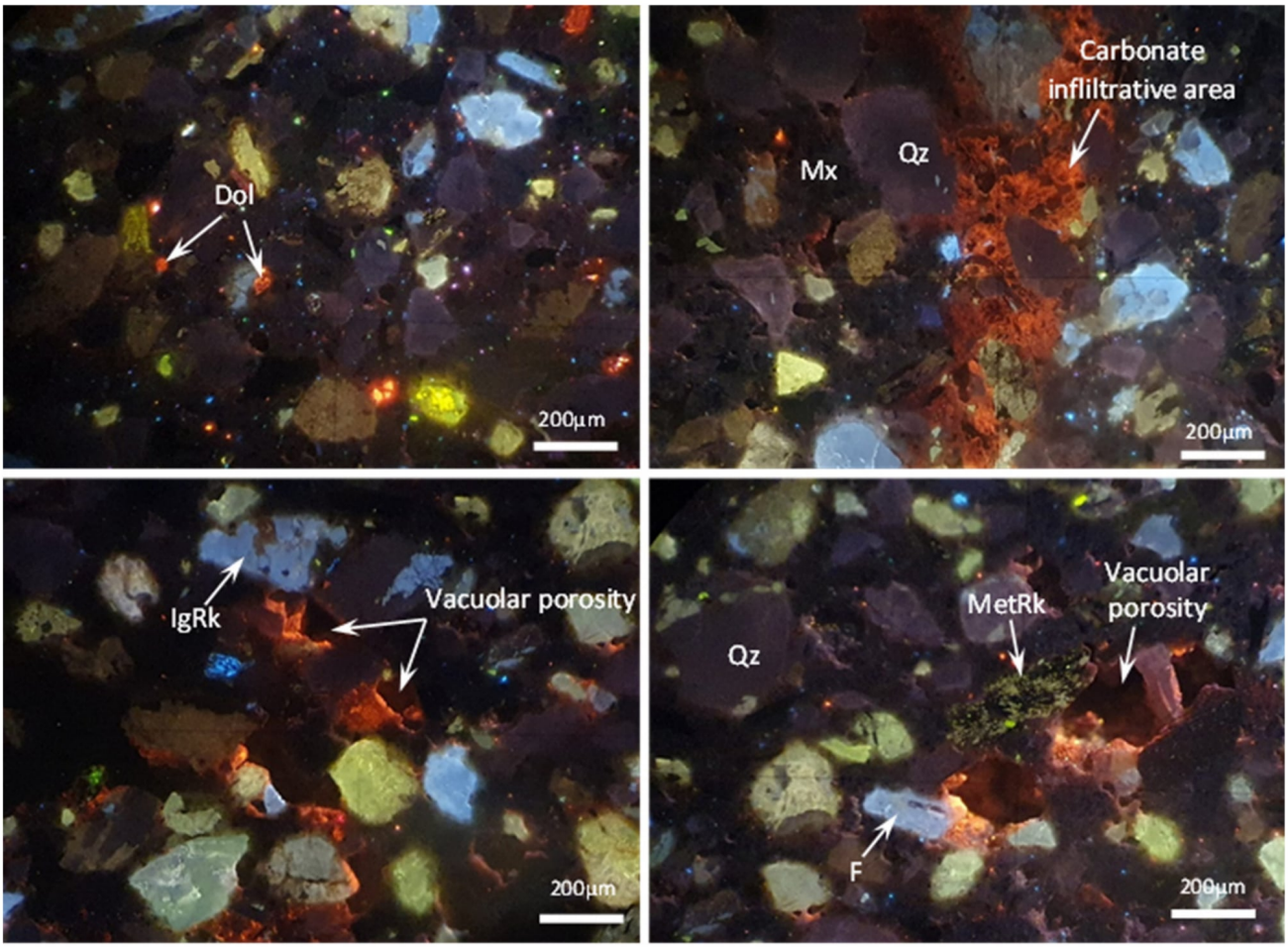

Figure 9. Microphotographs with external mortar of Corbii de Piatră. Qz—quartz. F—feldspar. IgRk—igneous rock fragment. MetRk—metamorphic rock fragments. Dol—dolomite crystals. Mx—matrix.

The microstructure exhibits fine, discontinuous cracks that are not interconnected and therefore do not contribute to water transport through the thickness of the mortar. The pores present in the mortar generally have rounded edges (Figures 10 and 11). In the void areas, crystal growth morphologies are observed during carbonation, where the crystal development occurred freely, protected from interaction with other aggregates (Figures 12 and 13).

The SEM–EDS elemental chemical composition at 13 points within the mortar (Figure 14, Table 2) provides information on the nature of the constituents.

The exterior mortar from Corbii de Piatră is atypical of lime mortars, both in terms of its morphology, characterized by large aggregates, and its composition. The point–scan SEM–EDS analysis of the mortar area (Figure 14, Table 2) reveals a heterogeneous microstructure consisting of a calcium-rich carbonate matrix associated with silicate particles derived from the sand aggregate. The composition suggests the presence of a common mineralogical background overlain by compositional variations. The high Fe contents (spectra 1, 7, 8, and 12) and Al contents (spectra 1, 2, 4, 7, 11, and 12) indicate the use of raw materials containing iron-bearing impurities and aluminosilicates. Spectra 1 and 7 indicate the presence of iron-rich inclusions, which may represent ferrous mineral fragments within the aggregate. The characterization also reveals high carbon contents (spectra 4, 5, 6, 10, 11, and 13), which may originate from fine charcoal particles. The areas exhibiting high Ca concentrations (spectra 8, 12, and 13) correspond to the carbonated lime binder, whereas spectra 2, 3, 4, 10, and 11 are characteristic of silicate aggregates. Overall, the data suggest the use of a

natural polymineralic aggregate in the preparation of a mortar based on carbonated air lime [53–56].

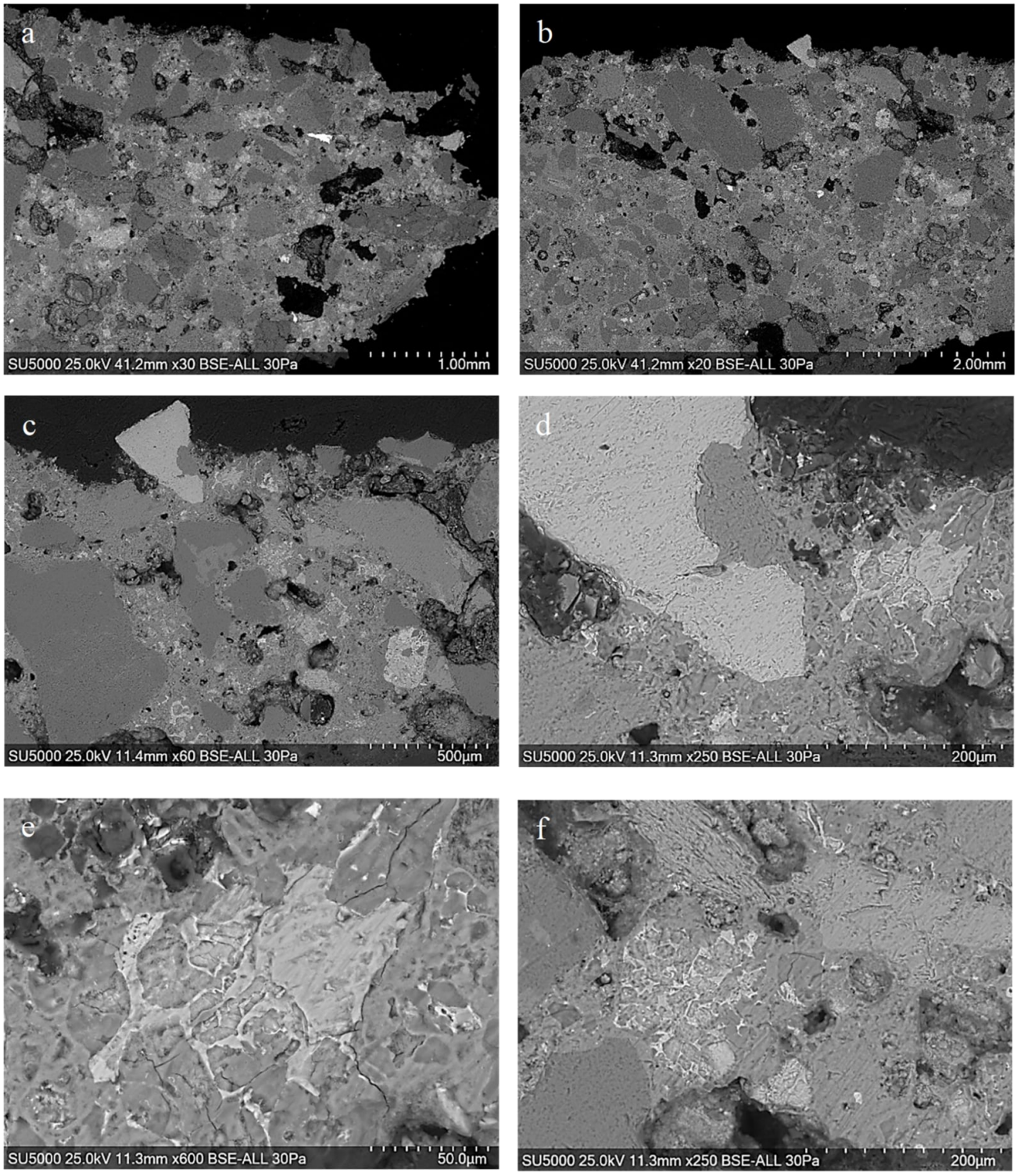

Figure 10. Cross-section SEM images of the Corbii de Piatră mortar: (**a**–**c**) fracture surfaces, large aggregates, and pores; (**d**–**f**) large aggregates and distinctive structural features.

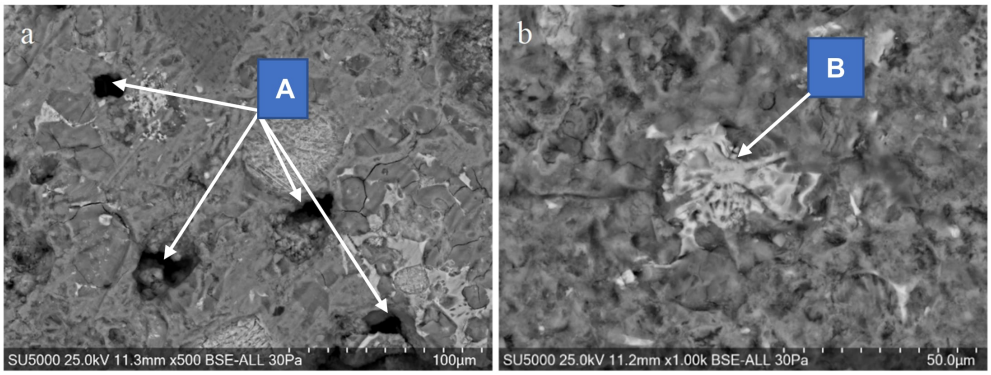

Figure 11. Lime-based mortar: (**a**) pores (A) and (**b**) rosette-like growth structures (B).

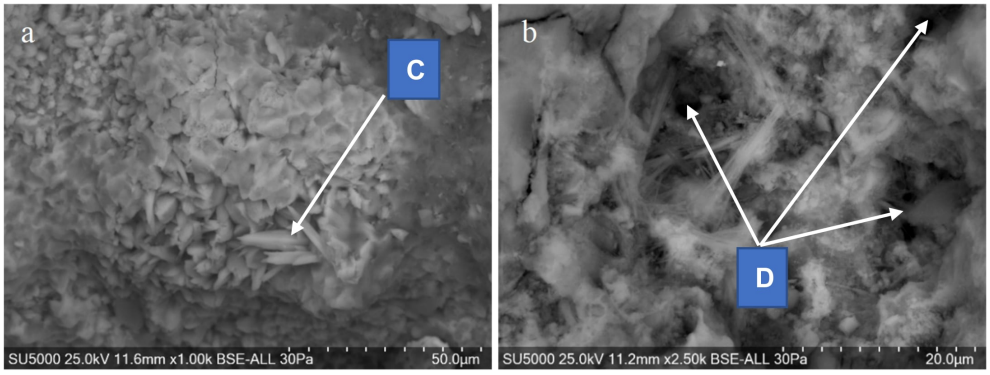

Figure 12. Spatial developments and (**a**) acicular growth of the mortar (C) (**b**) within voids (D).

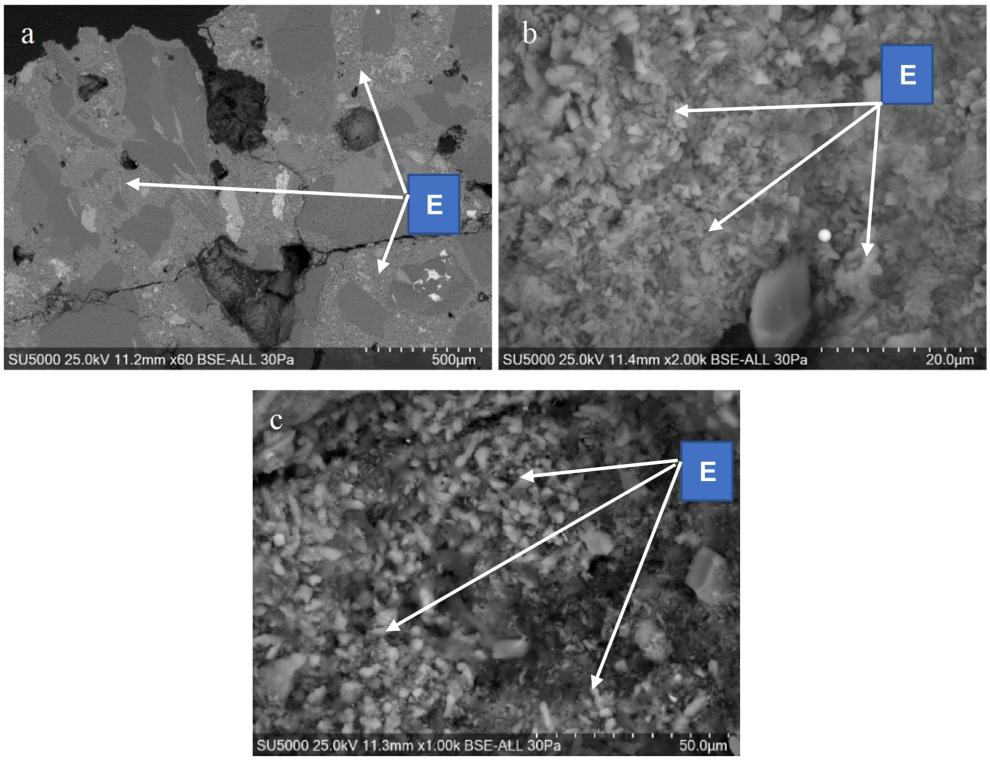

Figure 13. Crystal growth formations (E) within the mortar presented for different magnifications (**a**) 60×, (**b**) 2000×, (**c**) 1000×..

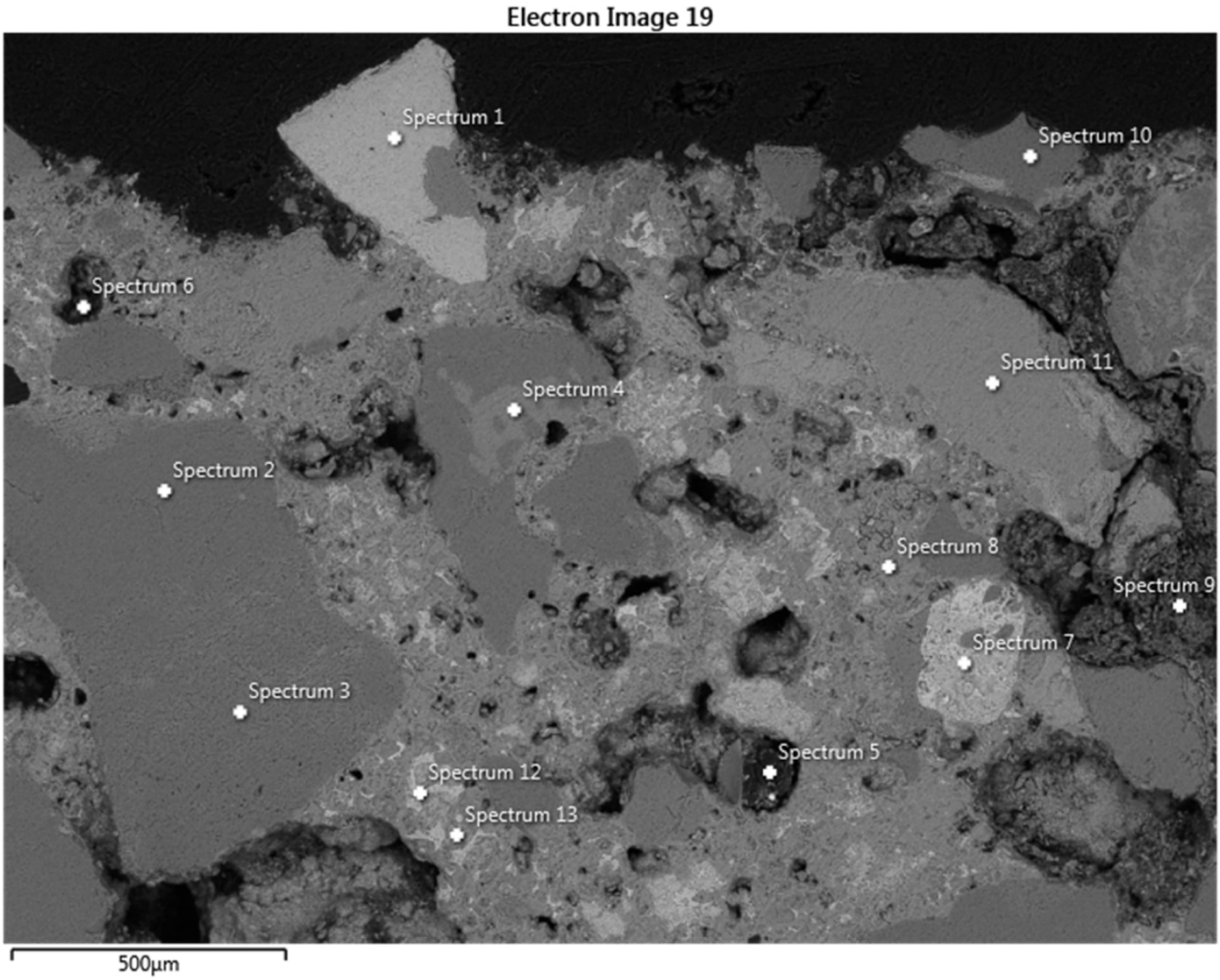

Figure 14. Cross-section SEM micrograph of the Corbii de Piatră mortar and SEM–EDS point–scan positions.

Elemental chemical composition map of a lime-rich area (Figure 15) highlights the sand particles (Si) embedded in the lime matrix, as well as the presence of aggregates rich in Fe, Na, K, and Mg, consistent with the cathodoluminescence analysis.

The presence of sulfur could be explained by its interaction with meteoric water, which washes the slopes formed by sulfur-rich sandstones. Sulfur occurs only at certain locations and in concentrations not exceeding 0.20 wt%. The high carbon content on the surface is attributed to external pollution. Small carbon-rich zones are also present within the mortar, as revealed by point spectral analysis.

The significant presence of iron, aluminum, and magnesium originating from the minerals contained in the aggregates used for mortar production is highlighted by the elemental chemical mapping, where these elements occur either as polyhedral constituents (Figures 15 and 16) or as constituents displaying a rosette-like morphology (Figures 17 and 18) [57,58].

Qualitative phase analysis by X-ray diffraction revealed the presence of Na and K together with Al in albite, muscovite, and sylvite (Figure 19, Table 3).

Qualitative phase analysis by X-ray diffraction (Figure 19, Table 3) identified quartz and calcite as the main crystalline phases, together with albite, muscovite and dolomite, and traces of gypsum.

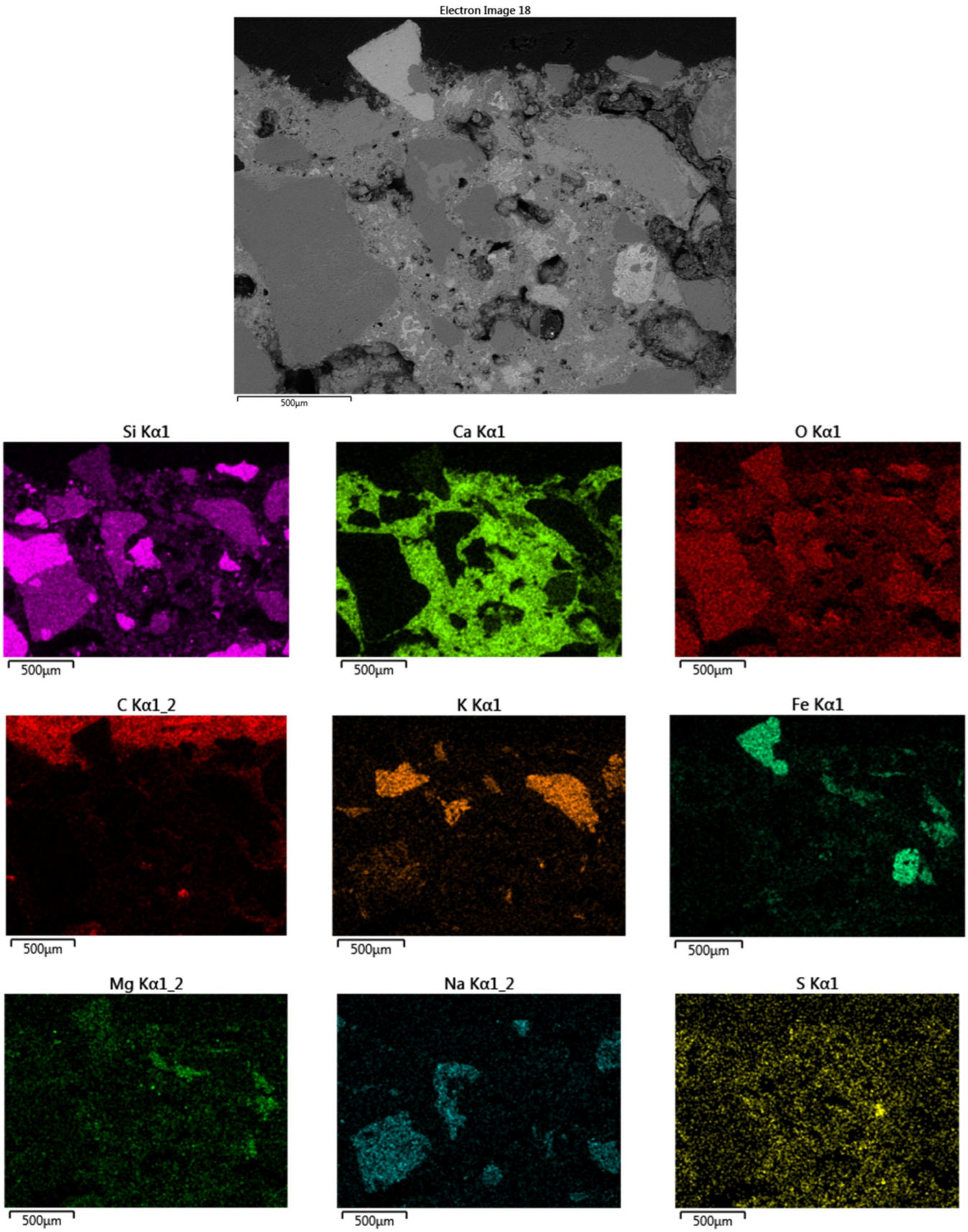

Figure 15. Cross-section SEM–EDS mapping of elemental chemical composition.

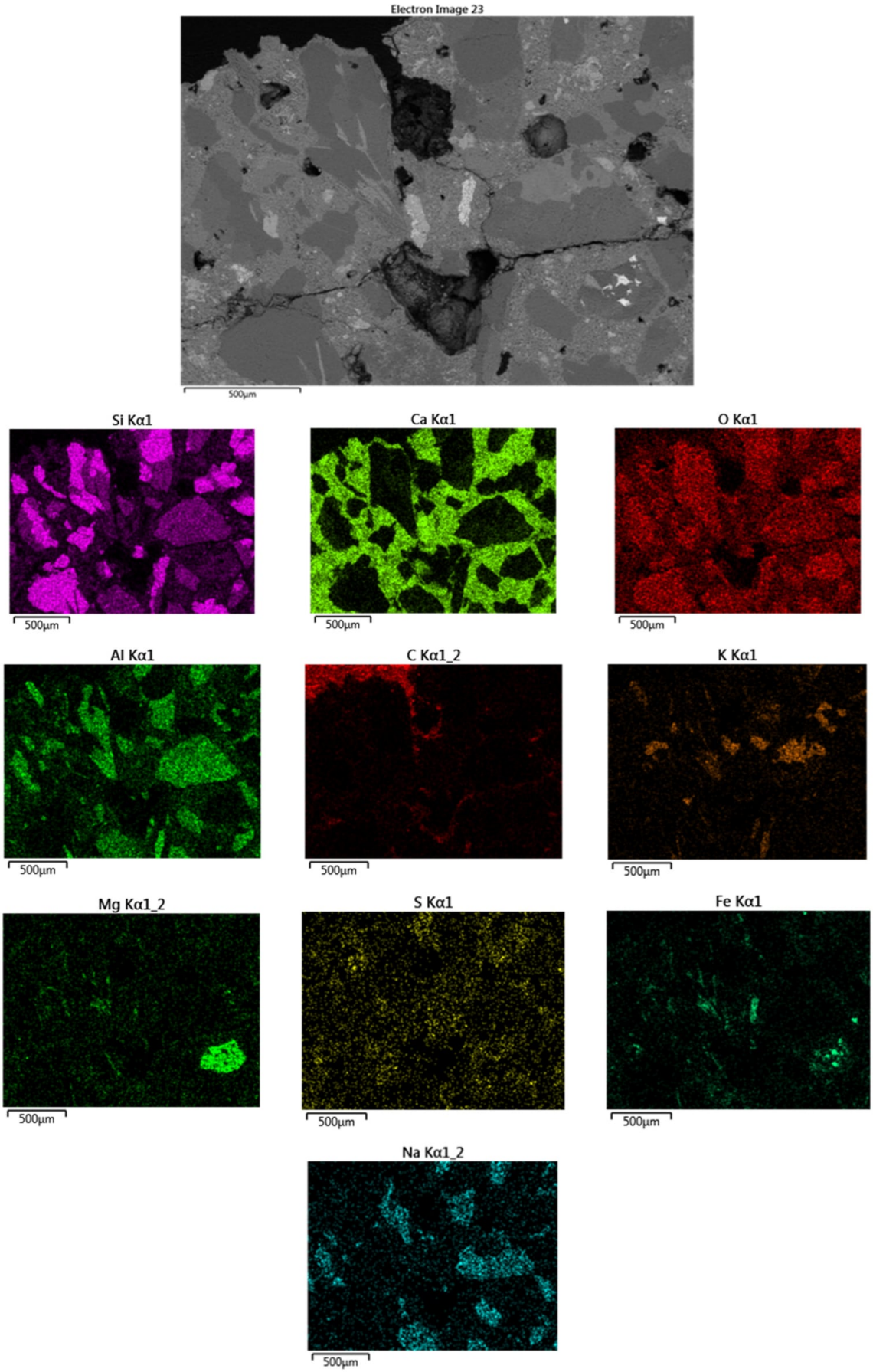

Figure 16. Cross-section SEM–EDS mapping on a fractured area.

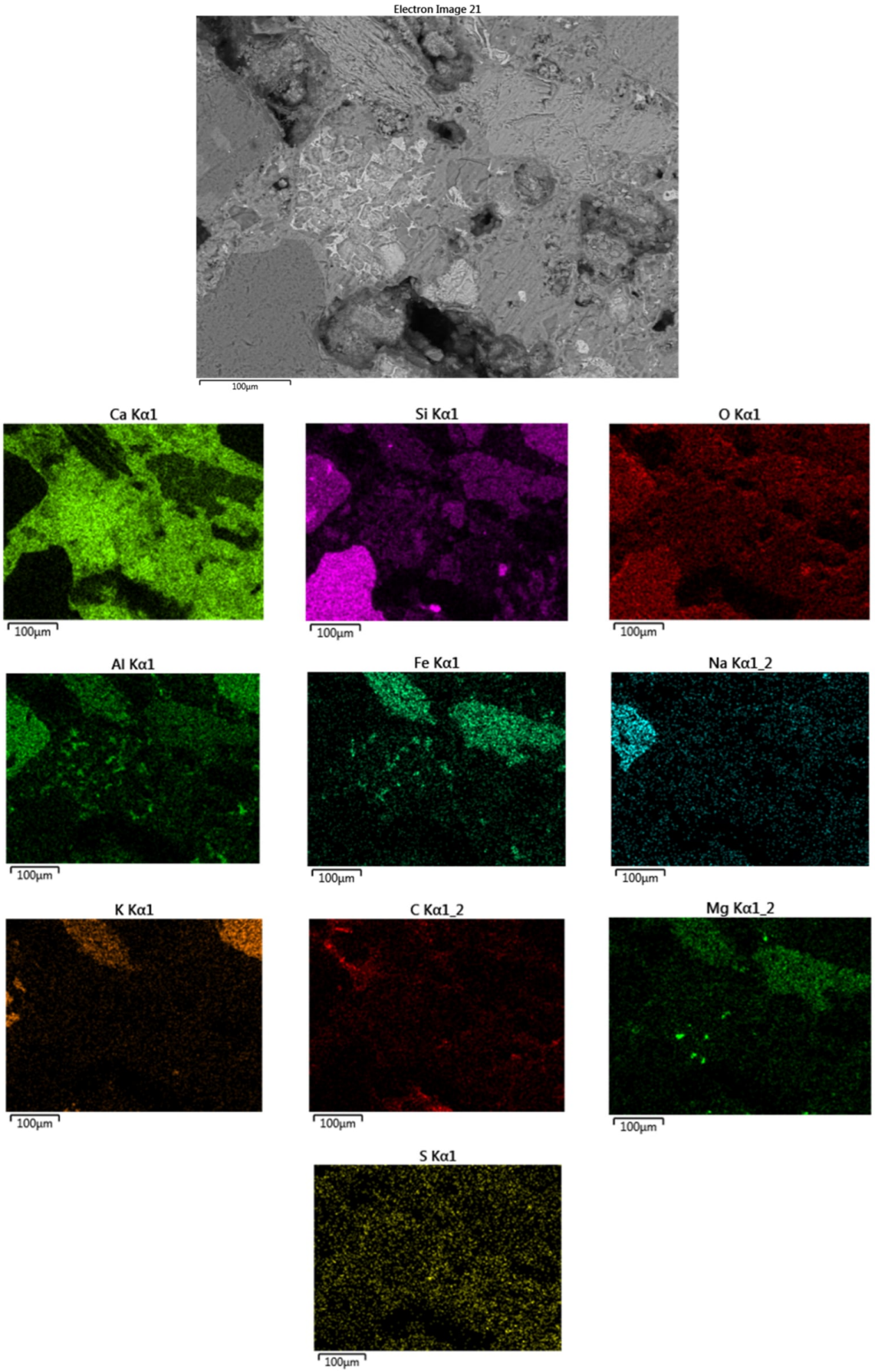

Figure 17. Cross-section SEM–EDS mapping on an area enriched in Al and Fe.

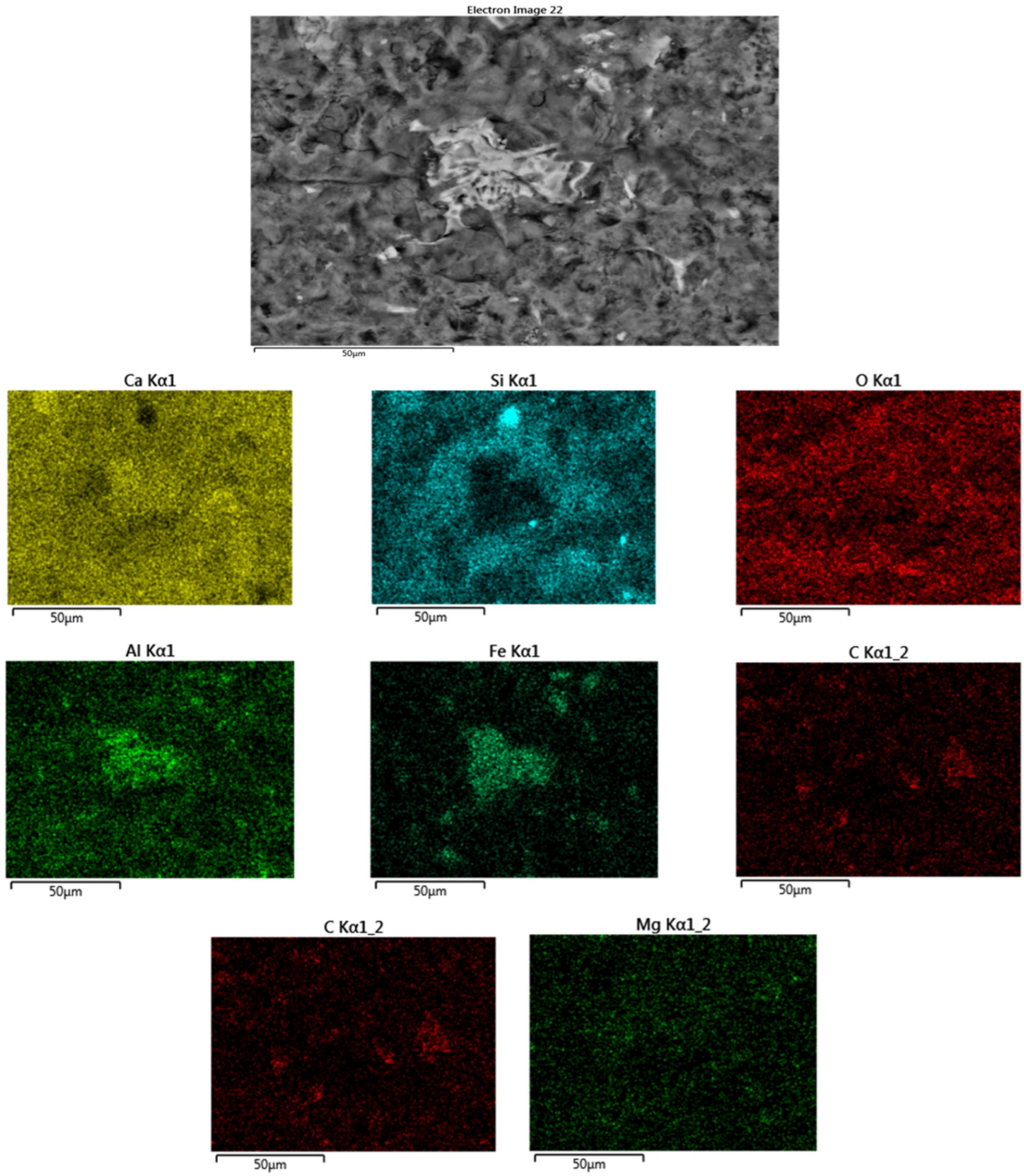

Figure 18. Cross-section SEM–EDS mapping on an area with a rosette-like structure.

Since the main gypsum reflection (~11.6° 2θ) and the low-angle reflections of clay minerals lie outside the measured 15–100° 2θ range, the identification of gypsum is tentative; a low-angle XRD analysis is recommended for future investigations.

The semi-quantitative phase composition, obtained by the Reference Intensity Ratio (RIR) method, is presented in Table 4. The dominant phase is quartz (56 ± 2 wt%), followed by calcite (27.0 ± 1.4 wt%), which represents the carbonated lime binder. Albite (7.3 ± 1.4 wt%) and muscovite (6.0 ± 0.7 wt%) are minor constituents of the aggregate, dolomite is present in a smaller amount (3.8 ± 1.1 wt%), and gypsum appears only in traces (0.4 ± 0.2 wt%). Assuming that the calcite originates mainly from the binder, the

binder-to-aggregate mass ratio is approximately 1:2.7, which is close to the 1:3 proportion typical of traditional lime mortars.

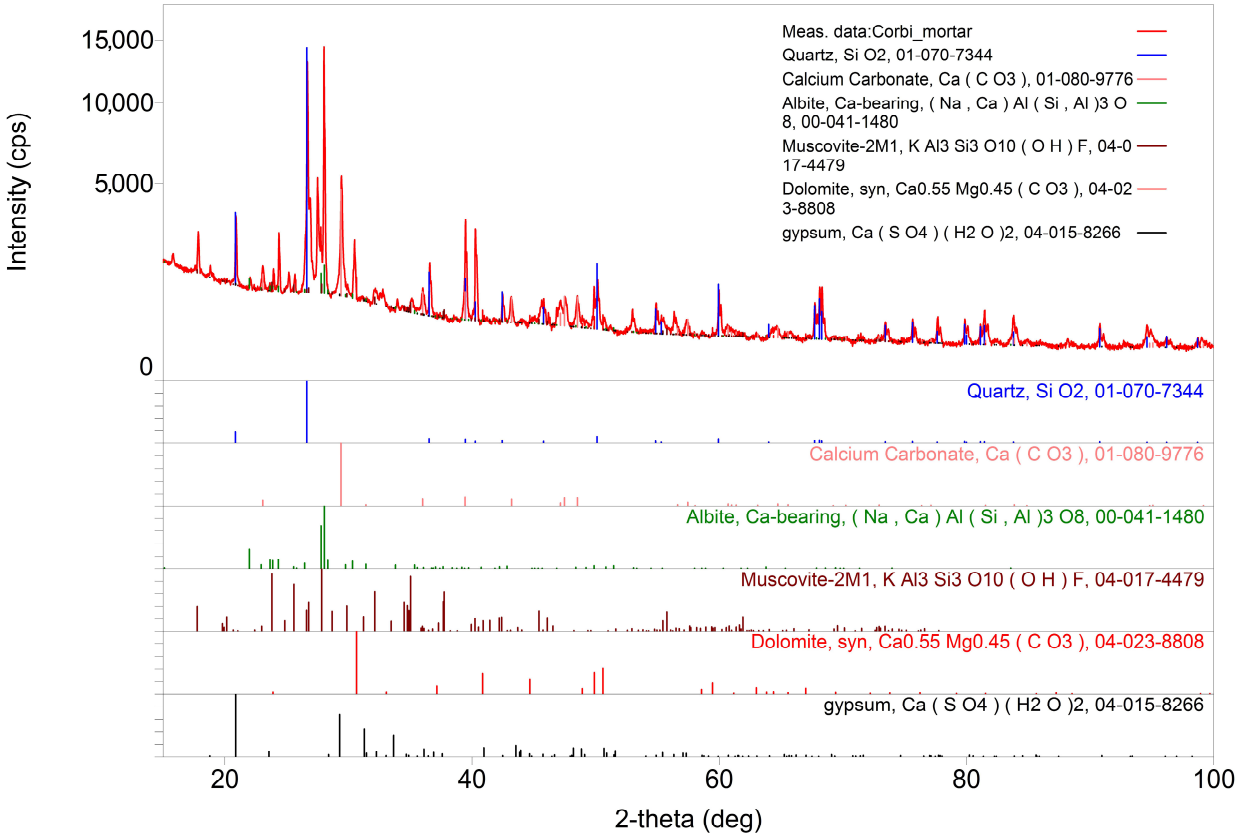

Figure 19. XRD qualitative phase analysis of the mortar (measured range 15–100° 2θ; the 20–70° region is shown).

Table 3. Phases identified in the mortar by qualitative X-ray diffraction analysis.

Phase Name	Formula	Figure of Merit	Phase Reg. Detail	DB Card Number
Quartz	SiO_2	0.867	ICDD (PDF-5+ 2024)	01-070-7344
Calcium Carbonate	$Ca(CO_3)$	1.034	ICDD (PDF-5+ 2024)	01-080-9776
Albite, Ca-bearing	$(Na,Ca)Al(Si,Al)_3O_8$	1.674	ICDD (PDF-5+ 2024)	00-041-1480
Gypsum	$Ca(SO4)(H_2O)_2$	2.925	ICDD (PDF-5+ 2026)	04-015-8266
Dolomite, syn	$Ca_{0.55}Mg_{0.45}(CO3)$	3.036	ICDD (PDF-5+ 2026)	04-023-8808

Qualitative phase analysis by X-ray diffraction is presented in Figure 19.

The presence of quartz, albite and muscovite indicates the use of a river sand derived from metamorphic and/or granitoid rocks, consistent with the cathodoluminescence observations. Dolomite is consistent with the dolomite microcrystals and Mg-calcite observed by CL in vacuoles and along infiltration pathways. Mg-calcite was not detected as a separate phase: after correction for sample displacement, the calcite (104) reflection lies at about 29.39° 2θ, close to the position of pure calcite, indicating that Mg-calcite occurs only locally, in amounts below the XRD detection limit. The trace amount of gypsum is consistent with the low sulphur content measured by SEM–EDS and indicates that interaction with meteoric water has not led to significant sulphation of the lime binder.

The radiocarbon dating of the exterior mortar was carried out at the RoAMS Laboratory of the Horia Hulubei National Institute for R&D in Physics and Nuclear Engineering

(IFIN-HH) using the 1 MV HVEE Tandetron™ Accelerator Mass Spectrometry (AMS) system (High Voltage Engineering Europa B.V., Amersfoort, The Netherlands) following the analytical procedures described in previous studies [44–52].

Table 4. Semi-quantitative phases composition of the mortar (RIR method).

Phase Name	Content (%)
Quartz	56 ± 2
Calcium Carbonate	27.0 ± 1.4
Albite, Ca-bearing	7.3 ± 1.4
Muscovite-2M1	6.0 ± 0.7
Dolomite, syn	3.8 ± 1.1
Gypsum	0.4 ± 0.2

When dating the exterior mortar of Corbii de Piatră, the documents attesting to the history of the Corbii de Piatră Church from the 12th to the 16th centuries were taken into account [7–10]. Radiocarbon dating of the interior frescoes was carried out at IFIN-HH in 2024 and places the analyzed parts in the 14th century, with a first stage from the time of Voivode Basarab I the Founder (1310–1352) and a second stage represented by a restoration on the northern wall dated to the second half of the 14th century [5]. Previously, the dating of the wood of the refectory table was carried out at the same laboratory in 2015, as belonging to the period 1725–1813. It is prior to a later restoration marked by an inscription on the southern interior wall dated 1881 [5]. These elements are therefore in connection with the advanced characterization of the exterior mortar, presented previously. For this, the radiocarbon date is found in the histogram in Figure 20.

The result (Figure 20) indicates four probability ranges for the dating of the lime mortar belonging to the exterior northern wall of Corbii de Piatră Church: a 24% probability that the age falls within the interval calAD 1643–1697; a 50.1% probability that the age lies between calAD 1723–1814; a 5.7% probability corresponding to the interval calAD 1836–1880; and a 15.6% probability that the age extends over calAD 1912.

Among these, the only interval that represents the majority aligns with historical data and fits perfectly with the dating of the table in the refectory, is calAD 1723 (50.1%)–1814. The dating of the refectory table previously yielded the following calibrated intervals: calAD 1638 (29.0%) 1695; calAD 1725 (51.1%) 1813; calAD 1839 (0.6%) 1846; calAD 1852 (1.7%) 1877; and a 13.0% probability that the age is later than calAD 1916 [10]. This table and the two benches in the refectory were identified and described in a work by the historian Constantin D. Aricescu, dating from 1856, which concerns the history of the town of Câmpulung, as shortly presented in [8].

Regarding the selection of these dominant intervals, no interventions on the northern church exterior are known from the early centuries. The only documented intervention is associated with the donation made by the Nun Magdalina to Neagoe Basarab in 1517. According to the literature presented in Introduction [7–9], on this occasion, the original entrance on the natural northern rock face was walled up, with access thereafter being provided from the southern side. The next recorded event is from 1809 when the site was transformed into a wedding church for Transylvanian emigrants arriving from across the mountains. Given that they settled here at the end of the 18th century, the interventions carried out can most likely be dated to the late 18th or early 19th century. Alternatively, they might be associated with the intervention of 1814—the excavation of the pronaos, the modification of the south side, and the reduction in the refectory area. Subsequent

interventions included the addition of the temple wall in 1819; the restoration of the west wall following its collapse in 1887; and the construction of a wooden belfry outside the cave area in 1890. Although the event of 1887 would be the most plausible candidate for dating the mortar on the exterior wall, none of the calibrated intervals encompass it and no historical record explicitly states that interventions took place on the northern side on that same occasion. No interventions to the exterior walls have been recorded since the beginning of the 20th century.

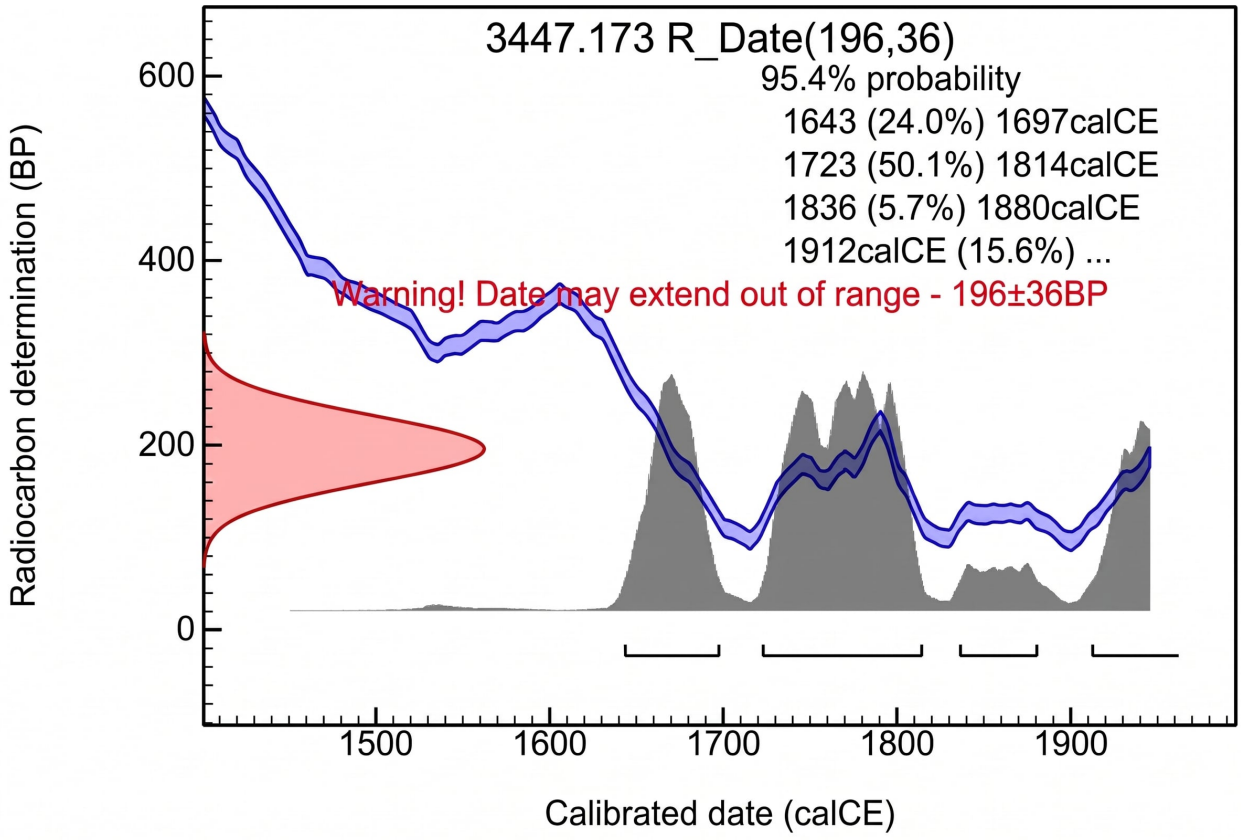

Figure 20. Calibrated radiocarbon probability distribution for mortar sample RoAMS-3447.173 (CRA = 196 ± 36 BP), calibrated using OxCal v4.4.4 and the IntCal20 atmospheric calibration curve [49,50]. The interval with the highest probability (50.1%) corresponds to the period 1723–1814 AD (cal). The probability intervals shown represent the 95.4% confidence interval.

Although the 17th-century period calAD 1643 (24.0%) to 1697 is also well represented, the lack of historical or archaeological evidence makes it less likely—though it should not be entirely ruled out.

4. Conclusions

The macroscopic analysis of the exterior mortar reveals the presence of large cracks, most likely associated with the expansion of ice in pores and micro-cracks occurring during repeated freeze–thaw cycles.

The mortar architecture ensures a good degree of compactness, giving the appearance of a well-set mortar, comparable to those used in ancient construction, characterized by fine porosity with predominantly non-interconnected pores.

Granulometric analyses of the mortar indicate the use of river sand as aggregate, with a particle size distribution dominated by medium-sized sand particles, in which larger aggregate particles are occasionally present.

The identified binder is of calcareous nature, consisting of air lime, with no additions of cement or other modern materials. Cathodoluminescence microscopic analyses reveal a homogeneous matrix with an advanced degree of carbonation, indicating a slow and natural setting process.

The cracks observed within the mortar mass are generally short, non-interconnected, and do not penetrate the entire thickness of the mortar layer, suggesting that meteoric water infiltration did not occur through the mortar matrix itself, but rather through the major cracks formed as a result of the expansion of ice in pores and micro-cracks during freeze–thaw processes.

Contact with meteoric water flowing over the sulfur-rich sandstone wall into which the church is carved has led to sulfur enrichment of the mortar matrix. However, due to the quality of the mortar and its high degree of compactness, interaction with meteoric water did not result in the development of significant compactness defects through the enlargement of pores or existing cracks that could constitute additional pathways for water infiltration toward the sandstone wall.

The results of the investigations suggest that the exterior mortar of Corbii de Piatră is a traditional material based on lime and natural aggregates, exhibiting adequate resistance to meteoric water transfer.

The composition and structure of the mortar indicate the use of a traditional technique characteristic of the historical period of the monument. The absence of cement and the presence of an air lime binder ensure good compatibility of the original mortar with modern lime-based restoration materials.

Radiocarbon data confirm the absence of geogenic calcite—or calcite resulting from recent recarbonation—within the extracted sub-micron fraction. The calibrated results yield multiple intervals. The primary sub-interval, calAD 1723 (50.1%) to 1814, aligns with historical documents or written accounts from the 19th century. A second, less probable sub-interval—calAD 1643 (24.0%) to 1697—is not supported by the recorded history of the cave complex. While it remains possible that future documentary discoveries might explicitly reveal when it was applied to the exterior wall, there is currently no evidence to support this. As for the 15.6% probability for the post-1912 period, the records concerning the Corbii de Piatră monastery complex are more numerous in this instance and show no such modern intervention applied to the northern wall within the investigated area.

The present interdisciplinary study focuses on the characterization of the exterior mortar of the Corbii de Piatră Cave Church, thereby complementing the results previously reported on the characterization of the fresco mortar from the same church [5,6].

The information provided by the material characterization supports the adoption, in the restoration of the church exterior, of a natural lime-based mortar compatible with the existing one, as well as the respect of traditional application techniques specific to the period, in order to avoid physico-chemical incompatibilities that could lead to accelerated deterioration.

Considering the wall's direct exposure to rainwater carried by the Cascade Stream, the use of a sacrificial lime mortar is recommended during restoration works to ensure long-term protection.

Author Contributions: Conceptualization, M.A., F.N.F. and D.A.N.; methodology, D.A.N., M.A., S.G.M. and D.G. software, F.P. and M.E.M.; validation, C.A.S., D.A.N., M.V.L.I. and M.A.; formal analysis, C.A.S., C.M., M.V.L.I., I.V.M., S.G.M. and D.A.N.; investigation: F.N.F., D.A.N., I.V.M., S.G.M., C.M., C.A.S., M.V.L.I., M.I.P., F.P., M.E.M., D.G., D.G.G., I.C.G., T.N.D., M.L. and M.A. resources, F.N.F. data curation, M.I.P., I.C.G., T.N.D., M.L. and D.G.G.; writing—original draft preparation, F.N.F., I.V.M., S.G.M., C.M., F.P., M.E.M., D.G. and M.A.; writing—review and editing and visualization,

D.A.N. and M.I.P.; supervision, M.A. All authors have read and agreed to the published version of the manuscript.

Funding: The radiocarbon dating was supported under Research Programme Partnership in Priority Areas PNII MEN-UEFISCDI, contract PN 23210102 and PN 23210201. Experiments were carried out at the 1 MV Tandetron™ accelerator from "Horia Hulubei" National Institute for R&D in Physics and Nuclear Engineering (IFIN-HH) and were supported by the Romanian Government Programme through the National Programme for Infrastructure of National Interest (IOSIN).

Institutional Review Board Statement: Not applicable.

Informed Consent Statement: Not applicable.

Data Availability Statement: All data results are in the present article.

Acknowledgments: We gratefully acknowledge the support of the Archdiocese of Argeș and Muscel and the Argeș County Directorate for Culture in facilitating the collection of samples.

Conflicts of Interest: The authors declare no conflicts of interest.

References

1. Corbii de Piatra. Available online: https://corbiidepiatra.ro (accessed on 20 November 2026).
2. Seclăman, M.; Bărzoi, S.C.; Luca, A.; Roban, R. *Corbii de Piatră. Interdisciplinary Study; Section. 2: Geological Characterization of the Site*; National University of Arts Printing: Bucureşti, Romania, 2010; ISBN 978-973-1922-98-0.
3. Cincheza-Buculei, E. *Corbii de Piatră. Interdisciplinary Study; Section. 1: Presentation of the Monument*; National University of Arts Printing: Bucureşti, Romania, 2010; ISBN 978-973-1922-98-0.
4. Mohanu, I.; Chatzitheodoridis, E.; Barbu, O.-H.; Niculescu, G.; Georgescu, M.; Şeclăman, M.; Bărzoi, S.-C.; Luca, A.; Roban, R. *Corbii de Piatră. Interdisciplinary Study; Section. 4: Technological Study of the Constituent Materials of Mural Painting*; National University of Arts Printing: Bucureşti, Romania, 2010; ISBN 978-973-1922-98-0.
5. Abrudeanu, M.; Simion, C.A.; Valcea, A.E.; Ilie, M.V.; Ispas, E.A.; Marin, M.L.; Mirea, D.A.; Olteanu, D.C.; Manailescu, C.; Petre, A.R.; et al. Radiocarbon Dating of Mortar Fragments from the Fresco of a Romanian Monastery: A Field Study. *Materials* **2025**, *18*, 1149. [CrossRef] [PubMed]
6. Vâlcea, A.E.; Mariș, I.; Negrea, A.D.; Cimpoeșu, N.; Gârbea, G.; Grecu, D.; Moga, S.G.; Istrate, B.; Finta, F.N.; Rizea, A.D.; et al. Mircea Ionuț Petrescu and Mărioara Abrudeanu: Interdisciplinary research on a medieval fresco mortar subjected to degradation processes in the Corbii de Piatră cave church. *Materials* **2023**, *16*, 5257. [CrossRef] [PubMed]
7. Dumitrescu, C.L. *Corbii de Piatră Rock Church, the Oldest Group of Paintings—Known Today—From Romania*; Art History Studies and Research; Romanian Academy Publishing House: Bucharest, Romania, 1975; Volume 22.
8. Ilinescu, I.; Gorunescu, I.; Şerban, I.-A. *Monastery of Corbii de Piatră*; History Pages; S.C. Zodia Gemenilor S.R.L.: Argeș, Romania, 2009.
9. Ştefănescu, I.D. *La Peinture Religieuse en Valachie et en Transylvanie Depuis les Origines Jusqu' au XIXe Siècle*; P. Geuthner: Paris, France, 1932; ISBN 978-2-7053-1015-8.
10. *Research Report on the Sample "Manastirea Corbii de Piatra, Argeș County" (RoMAG-30/32)*; Research Report No. 7/2015; Horia Hulubei National Institute for R&D in Physics and Nuclear Engineering (IFIN-HH): Măgurele, Romania, 2015.
11. Marincas, O. Contribution of the George Enescu Iasi University of Arts to the Interdisciplinary Research Project of Historical Monuments in Romania Undergoing Restoration. Available online: https://www.revistamonumenteloristorice.ro/fisiere/RMI_2008_1-2-010.pdf (accessed on 2 November 2026).
12. Characterization and Microanalysis of Ancient and Modern Materials by Physico-Chemical Methods. Laboratoire Scientifique Dédié à la Datation, L'analyse et la Characterisation des Materials et des Artefacts Archéologiques. Available online: https://www.archeophile.com/rwcat_129-laboratoires.htm (accessed on 2 November 2026).
13. G. LAMOA: Étude des Peintures Murales Avant la Restauration. Available online: https://www.lamoa.fr/services_analyse_des_peintures_murales.html (accessed on 2 November 2026).
14. Shevchenko, D.; Sadovskaya, Y.; Shkondin, V.; Zhurbin, Y.; Ostrovsky, A. Rock-Cut Church Göreme 31 (Cappadocia, Turkey): New Data from the Study in Situ (2014–2015). *Scrinium* **2021**, *17*, 274–290. Available online: https://uchisarcappadocia.org/red-church/ (accessed on 2 November 2026). [CrossRef]
15. Krajcar Bronić, I.; Topić, N.; Radić, I.; Peković, Ž.; Sironić, A. Radiocarbon dating of St. Stephen's in Pustijerna church in Dubrovnik, Croatia. In Proceedings of the Conference: Balkan Archaeometry Symposium, Bucharest, Romania, 29–30 October 2012. [CrossRef]

16. Al-Bashaireh, K. Reconstructing the Chronology of Building the Southwest Church of Umm el-Jimal, Jordan by AMS Radiocarbon Dating of Mortar and Plaster. *Radiocarbon* **2024**, *66*, 1–17. [CrossRef]
17. Kootahi, K.; Leung, A.K.; Jiang, Z.; Liu, Z.; Qi, R.; Lourenço, S.D.N.; Lai, Z.; Gao, Z. Evaluation of the Methods of Particle Morphology Characterization: CT Scanning, Digital Imaging and Light Microscopy. *Comput. Geotech.* **2024**, *174*, 106648. [CrossRef]
18. Gao, L.; Wang, D.; Miao, Y. A review of two-dimensional image-based technologies for size and shape characterization of coarse-grained granular soils. *Powder Technol.* **2024**, *445*, 120115. [CrossRef]
19. Mohanu, I.; Georgescu, M.; Mohanu, D.; Radu, L. Physical, mechanical and aesthetic characteristics of some mortars based on the lime–limestone–meta-argilite system. *U.P.B. Sci. Bull. Ser. B* **2012**, *74*, 85–96.
20. Pokrovsky, O.S.; Golubev, S.V.; Schott, J. Calcite, dolomite and magnesite dissolution kinetics in aqueous solutions at acid to neutral pH, 25 to 150 °C and 1 to 55 atm pCO2: New constraints on CO2 sequestration in sedimentary basins. *Chem. Geol.* **2009**, *265*, 20–32. [CrossRef]
21. Chapoulie, R.; Delery, C.; Daniel, F.; Vendrell-Saz, M.; Seca, C. Ceramics from Al-Andalus, Islamic Spain and Portugal Investigation with Sem–Edx and Cathodoluminiscence. *Archaeometry* **2016**, *47*, 519–534. [CrossRef]
22. Odelli, E.; Volpintesta, F.; Raneri, S.; Lefrais, Y.; Beconcini, D.; Palleschi, V.; Chapoulie, R. Digital image analysis on cathodoluminescence microscopy images for ancient ceramic classification: Methods, applications, and perspectives. *Eur. Phys. J. Plus* **2022**, *137*, 611. [CrossRef]
23. Milanesio, E.; Storta, E.; Gambino, F.; Appolonia, L.; Borghi, A.; Glarey, A. Petrographic characterization of historic mortar as a tool in archaeologic study: Examples from two medieval castles of Aosta Valley, Northwestern Italy. *J. Archaeol. Sci. Rep.* **2022**, *46*, 103719. [CrossRef]
24. *EN 12407:2019*; Natural Stone Test Methods—Petrographic Examination. European Committee for Standardization: Brussels, Belgium, 2019.
25. *SR EN 932-3:2022*; Tests for General Properties of Aggregates—Part 3: Procedure and Terminology for Simplified Petrographic Description. Asociația de Standardizare din România: Bucharest, Romania, 2022.
26. *EN 16515:2015*; Conservation of Cultural Heritage—Guidelines to Characterize Natural Stone Used in Cultural Heritage. Asociația de Standardizare din România: Bucharest, Romania, 2015.
27. Wenthorth, K.C. A Scale of Grade and Class Terms for Clastic Sediments. *J. Geol.* **1922**, *30*, 377–392. [CrossRef]
28. Maragh, J.M.; Palkovic, S.D.; Shukla, A.; Büyüköztürk, O.; Masic, A. SEM-EDS and microindentation-driven large-area high-resolution chemomechanical mapping and computational homogenization of cementitious materials. *Mater. Commun.* **2021**, *28*, 102698. [CrossRef]
29. Degloorkar, N.K.; Pancharathi, R.K. Characterization of ancient mortar for sustainability of an 800 year old heritage site in India. *Mater. Today Proc.* **2020**, *32*, 734–739. [CrossRef]
30. Teodorescu, L.; Amara, A.B.; Cantin, N.; Chapoulie, R.; Ducu, C.; Ciuca, S.; Tulugea, C.; Terteci, C.; Abrudeanu, M. Characterization of Archaeological Artefacts Using Methods Specific to Materials Science: The Case Study of Dacian Ceramics from 2nd c. BC to 1st c. AD. *Materials* **2021**, *14*, 3908. [CrossRef] [PubMed]
31. Sanjurjo-Sánchez, J.; Trindade, M.J.; Blanco-Rotea, R.; Garcia, R.B.; Mosquera, D.F.; Burbidge, C.; Prudêncio, M.I.; Dias, M.I. Chemical and mineralogical characterization of historic mortars from the Santa Eulalia de Bóveda temple, NW Spain. *J. Archaeol. Sci.* **2010**, *37*, 2346–2351. [CrossRef]
32. Germinario, G.; Logidoice, A.L.; Mezzadri, P.; Di Fusco, G.; Ciabattoni, R.; Melica, D.; Calia, A. Integrated Investigations to Study the Materials and Degradation Issues of the Urban Mural Painting *Ama Il Tuo Sogno* by Jorit Agoch. *Sustainability* **2024**, *16*, 5069. [CrossRef]
33. Adriano, P.; Silva, S.; Veiga, M.R.; Mirão, J.; Candeias, A.E. The Importance of SEM-EDS Analysis in the Study of Old Mortars. *Microsc. Microanal.* **2008**, *14*, 57–60. [CrossRef]
34. Cantisani, E.; Fratini, F.; Pecchioni, E. Optical and Electronic Microscope for Minero-Petrographic and Microchemical Studies of Lime Binders of Ancient Mortars. *Minerals* **2022**, *12*, 41. [CrossRef]
35. Grămescu, A.M.; Isopescu, D.N.; Carazeanu Popovici, I.; Pericleanu, M.; Pericleanu, B.D.; Anghelescu, C.E.; Voicu, G.; Ghiga, D.A. Material and Structural Characterization of Historical Masonry: Analytical Framework for Restoration Planning: A Case Study. *Appl. Sci.* **2025**, *15*, 6176. [CrossRef]
36. Borsoi, G.; Silva, A.S.; Menezes, P.; Candeias, A.; Mirão, J. Analytical characterization of ancient mortars from the archaeological roman site of Pisões (Beja, Portugal). *Constr. Build. Mater.* **2019**, *204*, 597–608. [CrossRef]
37. Al-Tell, Y.; Al-Manaser, A.; Hamadneh, I.; Al-Qadi, Q.; Yaseen, N. Analysis Of Mortar Samples And Mineral Composition From Deir El-Kahf, Jordan. *Arqueol. Iberoamaricana* **2025**, *25*, 74–81. Available online: https://www.laiesken.net/arqueologia/archivo/2025/AI5509.pdf (accessed on 20 November 2026).

38. Scottish Lime Centre Trust. *Report on Mortar Analysis by X-Ray Diffraction (XRD)*; Fife Historic Buildings Trust: Fife, UK, 2019. Available online: https://fifehistoricbuildings.org.uk/wp-content/uploads/2019/09/Appendix-D-Mortar-analysis-reports.pdf (accessed on 20 November 2026).
39. Panayiotis Kakavas: Characterization of the Historical Mortars Concerning Ancient Monuments-Experimental Approach. *SSRN Electron. J.* **2022**. [CrossRef]
40. Shukla, S.; Singh, L.P.; Mittal, A.K. Dwelling the Heritage: Characterization of Lime Mortar and Bricks Used in Forest Research Institute, Uttrakhand, India. *Int. J. Conserv. Sci.* **2022**, *13*, 457–472.
41. Pelosi, C.; Agresti, G.; Andaloro, M.; Baraldi, P.; Pogliani, P.; Santamaria, U. The Rock Hewn Wall Paintings in Cappadocia (Turkey). Characterization of the Constituent Materials and a Chronological Overview. *E-Preserv. Sci. (E-PS)* **2013**, *10*, 99–108. Available online: https://www.morana-rtd.com/e-preservationscience/2013/Pelosi-01-06-2012.pdf (accessed on 22 November 2026).
42. Dupouy, J.-M. Les rayons X et l'étude des œuvres d'art. *J. DE Phys. IV Proc.* **1996**, *06*, C4-791–C4-808. [CrossRef]
43. Martinetto, P.; Rousselière, H.; Walter, P. Identifier les pigments et comprendre leurs propriétés à partir de la diffraction des rayons X. *Actual. Chim.* **2014**, *387–389*, 170–174.
44. Ghita, D.G.; Mou, D.V.; Dogaru, M.; Gugiu, M.M.; Popescu, I.V.; Dobrescu, S.; Călinescu, C.I.; Căta-Danil, G.; Enăchescu, M.; Mărginean, N.; et al. Improvements of the research infrastructure at the tandem laboratory in IFIN-HH. *AIP Conf. Proc.* **2013**, *1525*, 208. [CrossRef]
45. *SR EN 14630:2007*; Determination of Carbonation Depth in Hardened Concrete Using the Phenolphthalein Method. Romanian Standards Association (ASRO): Bucharest, Romania, 2007.
46. Lindroos, A.; Ringbom, A.; Heinemeier, J.; Hajdas, I.; Olsen, J. Delayed Hardening and Reactivation of Binder Calcite, Common Problems in Radiocarbon Dating of Lime Mortars. *Radiocarbon* **2020**, *62*, 565–577. [CrossRef]
47. Marcu-Istrate, D.; Stanciu, I.M.; Simion, C.A.; Sava, T.B.; Păcesilă, D.G.; Ioniță, A.; Dobrotă, S.O. The Fortress of the Teutonic Order in South-eastern Europe: Feldioara/Marienburg from Early Foundation to Present-Day; Preliminary Archaeometric Studies. *Archaeol. Anthropol. Sci.* **2026**, *18*, 118. [CrossRef]
48. Stan-Sion, C.; Enachescu, M.; Petre, A.R.; Simion, C.A.; Calinescu, C.I.; Ghita, D.G. A new and compact system at the AMS laboratory in Bucharest. *Nucl. Instrum. Methods Phys. Res. Sect. B—Beam Interact. Mater. At.* **2015**, *361*, 105–109. [CrossRef]
49. Ramsey, C.B. Radiocarbon calibration and analysis of stratigraphy: The OxCal program. *Radiocarbon* **1995**, *37*, 425–430. [CrossRef]
50. Reimer, P.J.; Austin, W.E.N.; Bard, E.; Bayliss, A.; Blackwell, P.G.; Ramsey, C.B.; Butzin, M.; Cheng, H.; Edwards, R.L.; Friedrich, E.; et al. The IntCal20 Northern Hemisphere Radiocarbon Age Calibration Curve (0–55) Kbp. *Radiocarbon* **2020**, *62*, 725–757. [CrossRef]
51. Calandra, S.; Barone, S.; Cantisani, E.; Caggia, M.P.; Liccioli, L.; Vettori, S.; Fedi, M. Radiocarbon dating of straw fragments in the plasters of St. Philip church in archaeological site Hierapolis of Phrygia (Denizli, Turkey). *Radiocarbon* **2023**, *65*, 323–334. [CrossRef]
52. Simion, C.A.; Stanciu, I.M.; Sava, T.B.; Pacesila, D.G. Radiocarbon dating of a sample of hydraulic mortar from Porolissum customs. *Rom. J. Mater* **2022**, *52*, 349–356. Available online: https://solacolu.chim.upb.ro/pg349-356.pdf (accessed on 20 November 2026).
53. Stefanidou, M.; Papayianni, I. The role of aggregates on the structure and properties of lime mortars. *Cem. Concr. Compos.* **2005**, *27*, 914–919. [CrossRef]
54. Pavía, S.; Toomey, B. Influence of the Aggregate Quality on the Physical Properties of Natural Feebly-Hydraulic Lime Mortars. *Mater. Struct.* **2008**, *41*, 559–569. [CrossRef]
55. Lanas, J.; Alvarez, J.I. Masonry repair lime-based mortars: Factors affecting the mechanical behavior. *Cem. Concr. Res.* **2003**, *33*, 1867–1876. [CrossRef]
56. Arizzi, A.; Cultrone, G. The influence of aggregate texture, morphology and grading on the carbonation of non-hydraulic (aerial) lime-based mortars. *Q. J. Eng. Geol. Hydrogeol.* **2013**, *46*, 507–520. [CrossRef]
57. Ponce-Antón, G.; Zuluaga, M.C.; Ortega, L.Á.; Jiménez Echevarría, J.; Alonso Fernández, C. Characterization of Historic Lime Mortars from the Arch of San Martin to Identify the Construction Phases of the City Wall of Burgos (Spain). *Minerals* **2024**, *14*, 147. [CrossRef]
58. Fort, R.; Varas-Muriel, M.J.; Ergenç, D.; Cassar, J.; Anastasi, M.; Vella, N.C. The technology of ancient lime mortars from the Żejtun Roman Villa (Malta). *Archaeol. Anthropol. Sci.* **2023**, *15*, 15. [CrossRef]

Disclaimer/Publisher's Note: The statements, opinions and data contained in all publications are solely those of the individual author(s) and contributor(s) and not of MDPI and/or the editor(s). MDPI and/or the editor(s) disclaim responsibility for any injury to people or property resulting from any ideas, methods, instructions or products referred to in the content.